

Properties of CVSO 30 from *TESS* measurements: probably a binary T Tauri star with complex light curves and no obvious planets

C. Koen[★]

Department of Statistics, University of the Western Cape, Private Bag X17, Bellville, 7535 Cape, South Africa

Accepted 2020 April 15. Received 2020 March 28; in original form 2020 February 12

ABSTRACT

‘*Transiting Exoplanet Survey Satellite*’ (*TESS*) photometry of CVSO 30 spanned 21.8 d, with a single large gap of 1.1 d. This allows alias-free determination of the two periodicities in the data. It is confirmed that both of these are non-sinusoidal: the dominant $P_1 = 0.4990$ d has two detectable harmonics and $P_2 = 0.4486$ d has seven. The large number of harmonics in the second periodicity characterizes a very complex light curve shape. One of the features in the light curve is a sharp dip of duration ~ 2 h: this is probably the source of the previously claimed planetary transit signature. The star is a member of a small group of T Tauri stars with complex light curves, which have recently been exhaustively studied using *Kepler* and *TESS* observations. The two non-commensurate periods are most simply interpreted as being from two stars, i.e. CVSO 30 is probably a binary.

Key words: stars: individual: CVSO 30 - stars: variables: T Tauri.

1 INTRODUCTION

The weak-lined T Tauri star CVSO 30 (aka 2MASS J05250755+0134243, PTFO 8-8695) was discovered by Briceño et al. (2005), during the ‘Centro de Investigaciones de Astronomía’ Variability Survey in Orion. Several thousand *R*-band photometric measurements of CVSO 30 were made by the Palomar Transit Factory (PTF). Van Eyken et al. (2012) extensively analysed these observations and found a periodicity of 0.4484 d (frequency 2.230 d^{-1}). The non-sinusoidal periodic variations did not repeat exactly from cycle to cycle, and included low-amplitude depressions with durations of ~ 2 h. Van Eyken et al. (2012) ascribed the dips to planetary transits, caused by a planet with orbital period identical to the stellar rotation period. They found that the 0.4484 d flux depression periodicity is somewhat obscured in the light curves by typical aperiodic T Tauri variability.

Koen (2015) obtained multifilter time series photometry of CVSO 30 over the course of a week and found no transits. Analysis of his own photometry, as well as the PTF observations and measurements obtained by the Catalina Sky Survey (CSS; e.g. Drake et al. 2014), led him to conclude that there was evidence for two distinct non-sinusoidal periodicities in these data. The second frequency was very close to a small integer number of cycles per day, but the exact value could not be determined due to the frequency aliasing resulting from the relatively short individual observing runs on the star. Both the amplitudes and shapes (i.e. relative amplitudes of the harmonic components) of the periodicities are variable, a fact established by comparing different photometric data sets.

Extensive monitoring by Raetz et al. (2016) revealed substantial changes in the shape of the transit-like fadings, and their occasional disappearance. An explanation for variability in transit morphology, in terms of misalignment between the planetary orbit and the equatorial plane of CVSO 30, was put forward by Barnes et al. (2013) (see also Kamiaka et al. 2015). A critique of this model was given by Yu et al. (2015), who instead propose three alternatives: star-spots, effects of the presence of an accretion disc, or occultations of an accretion hotspot. The authors favour the last model: for example, they write ‘...the starspot model has difficulty reproducing the observed duration and occasionally sharp ingress/egress of the fading events’, while the evidence for an accretion disc was considered not entirely convincing. Further criticism of the Barnes et al. (2013) model can be found in Howarth (2016).

True transit depths are, of course, wavelength independent. Multicolour observations by Onitsuka et al. (2017) of a fading event of CVSO 30 showed a strong colour dependence, with the depth increasing with wavelength. The authors consider the more likely explanation of the flux dips to be obscuration by a transiting dust cloud. Tanimoto et al. (2020) obtained 20 photometric runs on the star, spread over a period of almost 5 yr. Most of the observing was done simultaneously through an I_C optical filter and either a J or K_S near-infrared filter. The authors found that there could be as many as three light-curve depressions per 0.4484 d cycle of variation. Two of the dips (labelled ‘A’ and ‘B’) were seen to be directly adjacent in the light curves, together spanning roughly 20 per cent of the cycle (~ 2.2 h). The onset of the third dip (‘C’) followed about 0.45 cycle (~ 4.8 h) after the end dip B. The dip depths were consistently smaller in the infrared, marginally so for dip type B. Tanimoto et al. (2020) entertain four different explanations for each of the dips – hot or cool star-spots, dust obscuration, or a planetary transit. They

[★] E-mail: ckoen@uwc.ac.za

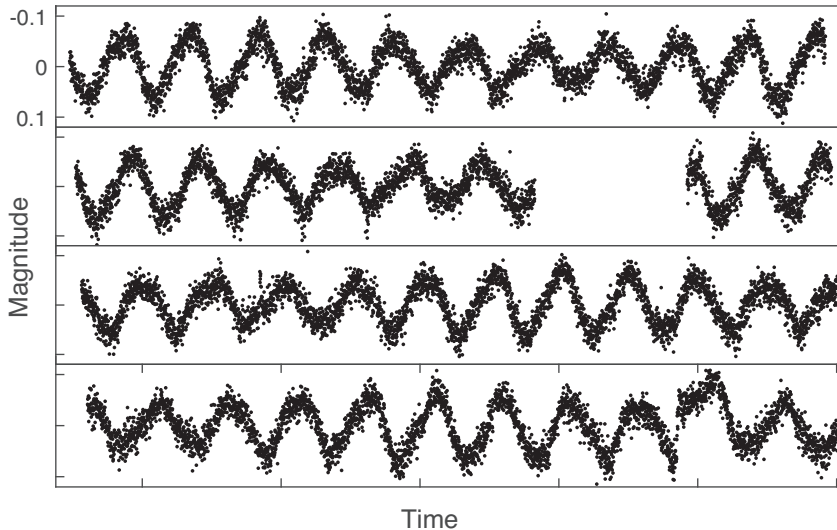


Figure 1. *TESS* photometry of CVSO 30. Each panel spans 5.7 d, and has a height of 0.24 mag.

concluded that dust is responsible for the A dips, a planet for the B dips, and less often observed C-type dips may result from either a hotspot or a dust cloud.

Variable $H\alpha$ emission of CVSO 30 was studied by Johns-Krull et al. (2016). The authors find correspondences between the positions of asymmetric features in the line profiles and the predicted planetary phase. Johns-Krull et al. (2016) posit that the excess emission is due to evaporation from a planet filling its Roche lobe. It should be noted though that the line profile asymmetries are primarily seen in their lower (2.6–8.7) signal-to-noise spectra.

A second planetary candidate (CVSO 30c) associated with the star was announced by Schmidt et al. (2016). The planetary status of this directly imaged object has been disputed by Lee & Chiang (2018).

The aim of this paper is to use the excellent precision of the *Transiting Exoplanet Survey Satellite* (*TESS* – Ricker et al. 2015) observations of CVSO 30 to

- (i) Resolve the aliasing of the frequency content of the light curves.
- (ii) Show that the transit-like feature may also be present in light curves where it is not evident, and that its shape mimics a sharp ingress and egress.
- (iii) Demonstrate that the morphology of the CVSO 30 light curve is very similar to that seen in a number of other T Tauri stars that exhibit complex periodicities, and occasionally second unrelated periodicities.

It will also be argued that the apparent absence of the transit-like feature or changes in its morphology may be simply due to changes in the relative amplitudes of the two periodicities. A similar argument applies to changes in spectral emission line profiles. Lastly, the wavelength dependence of the light-curve dips measured by Onitsuka et al. (2017) is compatible with the colour dependence of the light-curve amplitudes found by Koen (2015), i.e. the flux depressions simply scale with the light-curve amplitude at the particular wavelength.

2 FREQUENCY ANALYSIS

Two min cadence *TESS* observations of CVSO 30 were downloaded from the MAST (‘Mikulski Archive for Space Telescopes’) portal <https://mast.stsci.edu/portal/Mashup/Clients/Mast/Portal.html>. A few (nine) outlying values were removed from the PDCSAP (‘Pre-search Data Conditioned Simple Aperture Photometry’) flux measurements, leaving 14 818 observations, starting at JD 245 8468.2774 and spanning 21.77 d (Fig. 1). An amplitude spectrum of the data can be seen in the top panel of Fig. 2. It is dominated by the peak near 2.0 d⁻¹. Fitting a sinusoid to the data by least squares refined this to $f_1 = 2.0039$ d⁻¹. Subtracting the fitted sinusoid and calculating the spectrum of the residuals gave the result in the second panel: the largest peak is at 2.23 d⁻¹. Least-squares fitting gave the more precise value $f_2 = 2.2281$ d⁻¹. The two remaining panels of the figure show the effects of prewhitening also by f_2 and $2f_2$. The largest peak in the bottom panel is near 4 d⁻¹, the first harmonic of f_1 . Inspection of the spectrum indicates the presence of further harmonics of f_1 and f_2 .

Further prewhitening steps, followed by non-linear least-squares fitting, confirm the presence of two harmonics of f_1 and seven harmonics of f_2 in the data, with no further periodicities shorter than 0.5 d. Although there may be low-amplitude features with longer periods, the broad hump of excess power at the lowest frequencies is more suggestive of the presence of aperiodic variability, indicative of slight variations in instrument performance and/or data processing, or perhaps irregular T Tauri variability. Note that the general noise level is ~ 0.5 mmag for frequencies higher than 2 d⁻¹.

Formal error estimates of f_1 and f_2 are best obtained by simultaneously fitting sinusoids with the two frequencies with their harmonics, allowing the values of f_1 and f_2 to adjust so as to minimize the sum of squared residuals. The results are $f_1 = 2.0038 \pm 0.00011$ and $f_2 = 2.2292 \pm 0.00018$ d⁻¹. Note though that the precise solution is weakly dependent on starting guesses for the values of the estimated parameters – hardly surprising seeing that 2 frequencies, 11 amplitudes, and 11 phases are determined simultaneously. The corresponding periods are $P_1 = 0.49905 \pm 2.7 \times 10^{-5}$ and $P_2 = 0.44859 \pm 3.6 \times 10^{-5}$ d.

The CSS (Drake et al. 2014) observations of CVSO 30 span 7.8 yr, which is a longer time baseline than any other source of

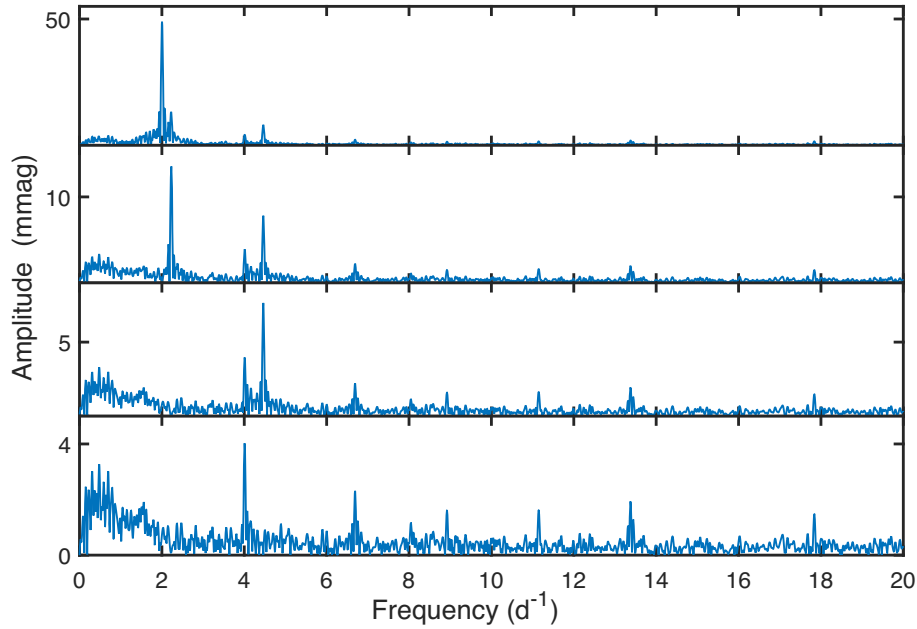


Figure 2. The top panel is an amplitude spectrum of the data in Fig. 1. The tallest peak is at a frequency of 2.00 d^{-1} . The remaining panels show amplitude spectra of the residuals after prewhitening by the dominant one, two, and three frequencies, respectively. Note the peaks at harmonic frequencies, most obvious in the bottom panel.

Table 1. Aside from some apparently aperiodic low-frequency features, the table gives the amplitudes (in mmag) of all discernible sinusoidal components in the *TESS* observations of CVSO 30. The formal error of all amplitudes is 0.22 mmag .

Frequency (d^{-1})	Harmonic number							
	0	1	2	3	4	5	6	7
$f_1 = 2.0038$	49.3	3.99	0.77	–	–	–	–	–
$f_2 = 2.2292$	13.5	7.61	2.30	1.63	1.67	1.92	0.38	1.43

homogeneous photometry of the star. It therefore also provides the most accurate determination of the variability frequencies, namely $f_1 = 2.00317 \text{ d}^{-1}$ and $f_2 = 2.22743 \text{ d}^{-1}$, both with formal standard errors of $2 \times 10^{-5} \text{ d}^{-1}$ (see Koen 2015). Note that in the case of f_2 , the largest spectral peak given by the Catalina data is at a 1 d^{-1} alias; this can now be unambiguously corrected since the *TESS* data are alias free. The corresponding periods are $P_1 = 0.49921 \pm 5.0 \times 10^{-6}$ and $P_2 = 0.448948 \pm 4.0 \times 10^{-6} \text{ d}$.

Formally, the two sets of frequency determinations above do not agree. This is most likely due to error estimates that are far too optimistic: in the case of the *TESS* data due to the simultaneous estimation of 24 parameters, and in the case of CSS due to the fact that many parameters are not modelled at all. Adequate error estimation when fitting time series models is a topic of ongoing research and outside the scope of this paper.

Table 1 gives a list of the amplitudes (A_j and B_k) of the harmonics of $f_1 = 2.0038$ and $f_2 = 2.2292 \text{ d}^{-1}$:

$$y(t) = y_1(t) + y_2(t) = \sum_{j=1}^3 A_j \cos[2\pi(jf_1 t + \phi_j)] + \sum_{k=1}^8 B_k \cos[2\pi(kf_2 t + \psi_k)]. \quad (1)$$

Fig. 3 demonstrates the very good fit to the observations.

In Fig. 4, the two individual components y_1 and y_2 in (1), and their sum y , are plotted. The diagram makes the point that since the model light curve y was dominated by the component y_1 during these observations, very little of the complexity of component y_2 is visible in their sum y . The situation would, of course, have been different had y_2 been more prominent. The contents of Table 2 provide an explanation of why flux depressions were readily found by Van Eyken et al. (2012), but seen in neither the observations of Koen (2015) nor the *TESS* data: the amplitude of the f_2 periodicity was largest during their observing campaigns.

Fig. 5 shows the y_2 light curve in more detail; a little more than two cycles of length $P_2 = 1/f_2 = 0.4488 \text{ d}$ (or 10.77 h) is plotted. Of particular importance is the deep feature near 4 h (repeated near 15 h); the width of the accompanying thick horizontal line is 2 h – the duration of the flux dips studied by Van Eyken et al. (2012). Note also the steep ‘ingress’ and ‘egress’ of the feature. The small bump in the middle of the depression has a height of $\sim 2 \text{ mmag}$, and would not normally be evident in photometry performed through the Earth’s atmosphere, particularly given the presence of the y_1 variation. None the less, inspection of fig. 8 in Van Eyken et al. (2012) does suggest a small flux increase mid-way through the dip in their phase-folded 2009 light curve; see also fig. 1 in Barnes et al. (2013).

The presence of the three different flux depressions (A, B, and C) described by Tanimoto et al. (2020) is also obvious in the *TESS* light

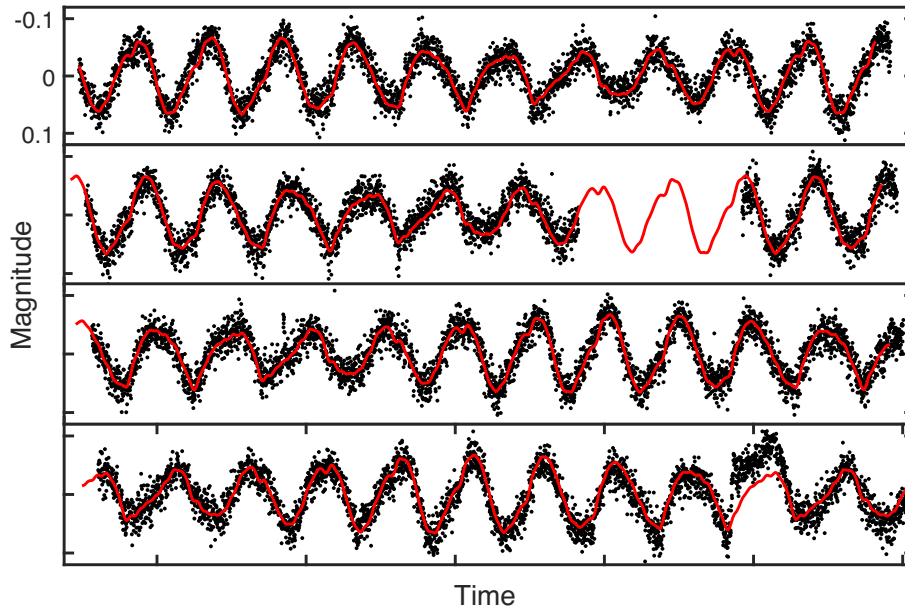


Figure 3. As for Fig. 1, but also showing a model fit consisting of sinusoids with frequencies f_1 (and its first two harmonics) and f_2 (and its first seven harmonics).

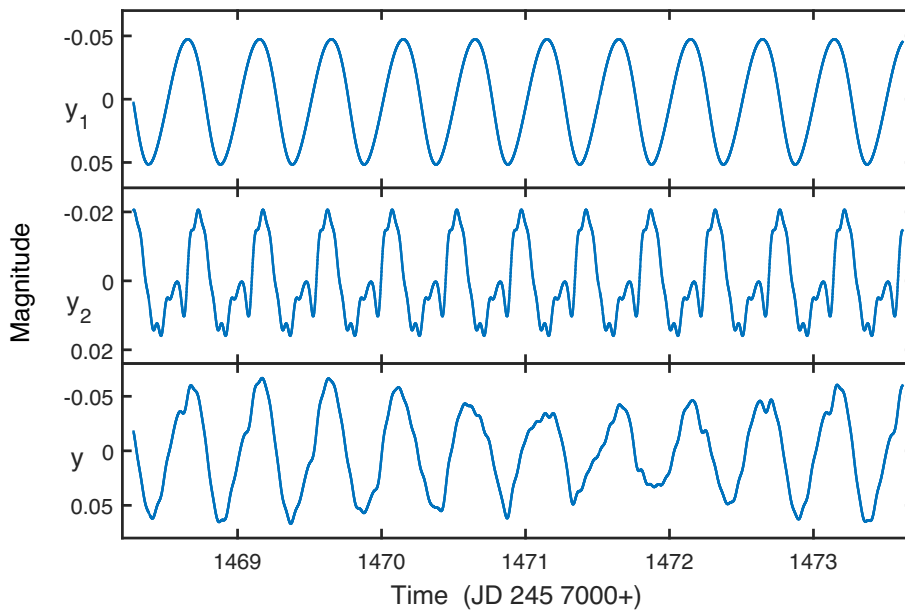


Figure 4. A decomposition of the model light curve fitted to the observations in the top panel of Fig. 3. Top panel: the non-sinusoidal periodicity with frequency f_1 and its first two harmonics. Middle panel: the non-sinusoidal periodicity with frequency f_2 and its first seven harmonics. Bottom panel: sum of the two periodicities plotted in the top two panels. See Table 1 for the amplitudes of the various components. Note the different scales on the vertical axes.

Table 2. A comparison of the amplitudes (in mmag) associated with f_1 and f_2 during various observing runs. Van Eyken et al. (2012) studied the star during two observing seasons (2009 and 2010) using an *R* filter, while Koen’s 2015 observations were taken contemporaneously through different filters.

Source	Van Eyken et al. (2012)		Koen (2015)		<i>TESS</i>
	2009	2010	R_C	I_C	
$f_1 = 2.0039$	42	28	31	16	49
$f_2 = 2.2281$	30	25	8	4	14

curves. Fig. 5 makes clear the danger of extracting specific features in isolation, and then considering separate physical explanations for each of these. It seems much more reasonable to look for a single mechanism, or combination of factors, which can give rise to such complicated light curves – an issue that we proceed to place in context.

It is of interest to compare Fig. 5 to the complex light curves of some T Tauri stars observed in detail by the *Kepler* and *TESS* missions. For convenience, this group of stars will be referred to in what follows as CLTTs (‘Complex Lightcurve T Tauri stars’).

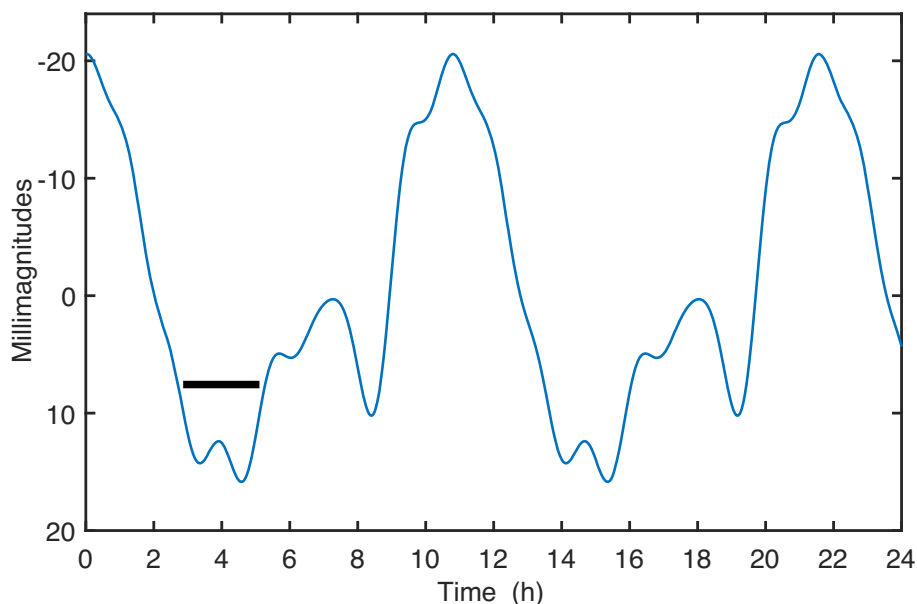


Figure 5. Details of the light curve y_2 in the middle panel of Fig. 4 (i.e. associated with f_2). The short horizontal bar indicates a time interval of 2 h.

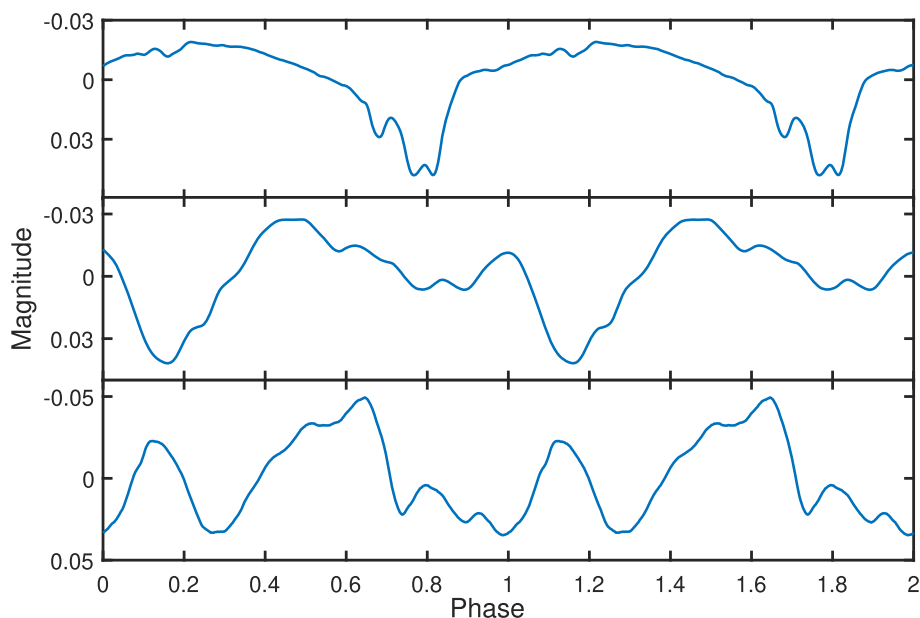


Figure 6. Three examples of complex short-period T Tauri star light curves. From top to bottom: TIC 224283342 ($P = 0.8873$ d), TIC 332517282 ($P = 0.4023$ d), and TIC 425937691 ($P = 0.2007$ d).

The reader is referred to Stauffer et al. (2017, 2018) and Zhan et al. (2019) for exhaustive discussions of CLTTs; in a nutshell, the periodicities in these stars are characterized by many harmonics of the fundamental frequency. Fig. 6 contains three example *TESS* light curves. These data were also downloaded from the MAST portal, phase folded with respect to the periods given in Zhan et al. (2019), and then smoothed. Clearly, CVSO 30 is no stranger in this company.

Some of the characteristics of the CLTT class are (Stauffer et al. 2017, 2018; Zhan et al. 2019): typical spectral types are M3.5–M5; ages are in the range 1–45 Myr; spectra show Li in absorption, $H\alpha$ emission; periods are shorter than 1 d; infrared excesses are uncommon; and secondary non-commensurate periodicities, ascribed

to binary companions, have been found in several CLTTs. As of writing this, only a few dozen of these stars have been described in the literature.

Consensus has not been reached about the variability mechanism in these stars. The obvious contender, given that these stars are T Tauris, is rotation coupled with star-spots. However, Stauffer et al. (2017) were unable to simultaneously produce the requisite light-curve shapes and amplitudes using star-spot models. Likewise, Zhan et al. (2019) could not reproduce the observed light curves with dark star-spots. Bright star-spots have been ruled out, as the lack of infrared excesses implies a lack of accretion material (Stauffer et al. 2017). Proposed models involve circumstellar gas (lost from the photosphere due to rapid rotation), or a combination

Table 3. Some physical properties of CVSO 30.

Source	A_V	T_{eff}	R/R_{\odot}	L/L_{\odot}	M_{bol}
Briceño et al. (2005)	0.12	3470	1.39	0.25	6.25
Briceño et al. (2019)	0.51	3415	–	–	–
This paper	0.24	3380	1.41	0.24	6.29

of star-spots and obscuration by circumstellar dust in an inclined disc.

3 SOME PHYSICAL PROPERTIES OF THE STAR

A *Gaia* parallax of 2.8614 ± 0.0751 mas (Gaia Collaboration 2018), as well as new photometry of CVSO 30, has become available since properties of the star were derived by Briceño et al. (2005). This new information is exploited in this section of the paper. The parallax measurement implies an absolute magnitude at wavelength λ of

$$M_{\lambda} = m_{\lambda} - 7.717$$

with an error of 0.057 mag (provided the error in m_{λ} is negligible). A number of apparent magnitudes are available in the literature: *VI*C (Briceño et al. 2005); Pan-STARRS *grizy* (Chambers et al. 2016); *Gaia* G , G_{BP} , and G_{RP} (Gaia Collaboration 2018); 2MASS JHK_S (Skrutskie et al. 2006); and WISE $W1$ and $W2$ (Cutri et al. 2014). Note that the WISE $W3$ filter measurement appears to be unreliable – it has a large error (0.14 mag), and is anomalously *fainter* than the $W1$ and $W2$ observations.

Bolometric magnitudes follow from the m_{λ} as

$$M_{\text{bol}} = M_{\lambda} + BC_{\lambda} = m_{\lambda} + BC_{\lambda} - 7.717.$$

Bolometric corrections BC_{λ} for all the filters are conveniently available from the ‘MESA Isochrones and Stellar Tracks’ website http://waps.cfa.harvard.edu/MIST/model_grids.html#bolometric. Applying the bolometric corrections requires the stellar temperature and gravity, but given that there are 15 distinct m_{λ} available to determine a single M_{bol} , the overdetermination can be used to obtain the

absorption A_V , T_{eff} , and $\log g$ together with M_{bol} by minimizing

$$S = \sum_{\lambda} [M_{\text{bol}} - (m_{\lambda} - A_V f_{\lambda} + BC_{\lambda} - 7.717)]^2.$$

The extinction $f_{\lambda} = A_{\lambda}/A_V$ was taken from Schafly et al. (2016).

The luminosity follows from the relation

$$M_{\text{bol}} = 4.74 - 2.5 \log(L/L_{\odot}) \quad (2)$$

and the stellar radius from

$$L = 4\pi R^2 \sigma T_{\text{eff}}^4, \quad (3)$$

where σ is the Stefan–Boltzman constant.

Relevant results are in Table 3, which compares present determinations to those by Briceño et al. (2005, 2019). The agreement is excellent, aside from A_V that is substantially different. It is noteworthy that the error on the present determination of M_{bol} is only 0.057 mag, dominated by the distance uncertainty. The individual estimates of M_{bol} (i.e. for each of the 15 filters) are plotted in Fig. 7; the standard deviation is 0.024 mag.

A criticism of the procedure above (specifically, the use of the bolometric correction tables) is that it may ignore differences between the colours of stars on the main sequence and T Tauri stars (e.g. Gullbring et al. 1998a,b). The de-reddened colours of CVSO 30 can be compared to those in the comprehensive compilation http://www.pas.rochester.edu/~emamajek/EEM_dwarf_UBV_IJHK_colors_Teff.txt (Pecaut, Mamajek & Bubar 2012; Pecaut & Mamajek 2013). This online table gives a wide variety of colour indices for all main sequence spectral types. Of these, nine indices involving the V , I_C , *Gaia*, 2MASS, and WISE filters can be used in the present context. Fig. 8 shows the root mean squared difference between the colours derived for CVSO 30 and those in the online table, for a range of spectral types. The minimum of 0.052 mag is at the spectral type M3, suggesting that the colours of the star are not systematically different from that of a main-sequence M3 star. Furthermore, given that the star is variable, the agreement between the de-reddened colours and the table values is good.

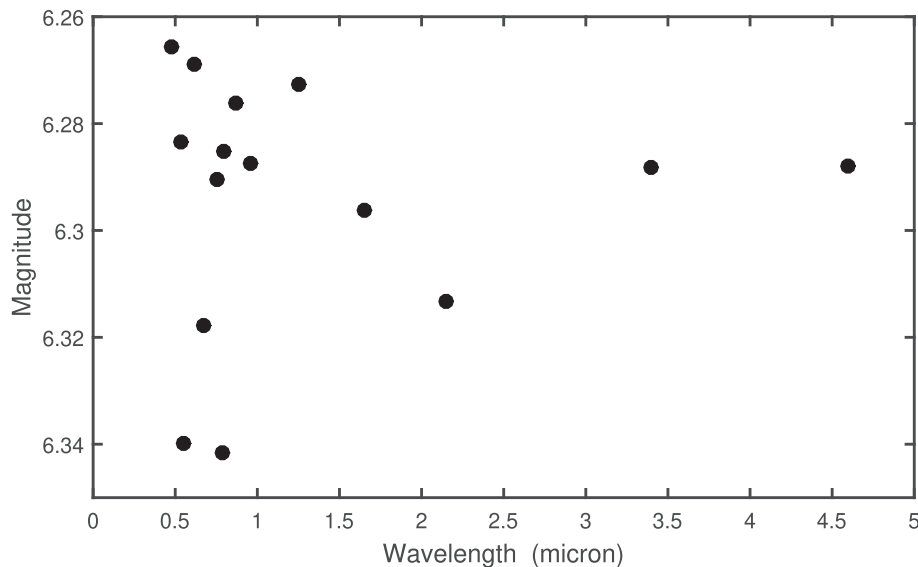


Figure 7. Estimates of the bolometric magnitude, based on 15 different apparent magnitudes from the literature. The effective wavelength of each filter is given on the horizontal axis.

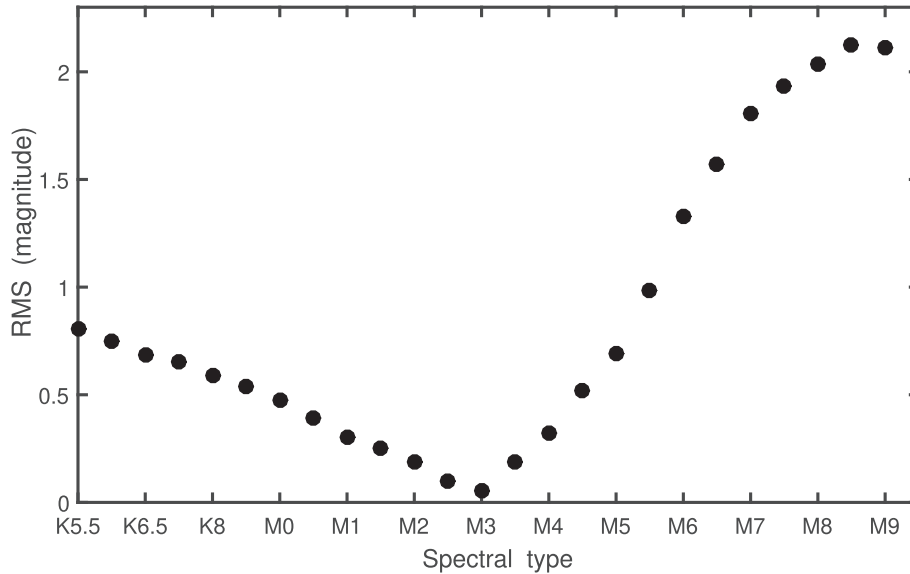


Figure 8. The discrepancy between the de-reddened colour indices of CVSO 30 and main sequence indices from Pecaut, Mamajek & Bubar (2012) and Pecaut & Mamajek (2013).

4 DISCUSSION

The most straightforward explanation for the two independent non-sinusoidal periodicities in CVSO 30 is that there are two stars involved. The fact that variability of both stars is discernible, and that the spectra do not show overt signs of binarity, suggests that the stars are of similar luminosities and spectral types. The absence of radial velocity variations of any substance (Van Eyken et al. 2012) implies that the star is not a short-period binary. Given that both periodicities are non-sinusoidal, it seems likely that both stars are T Tauris. It is noteworthy that several of the CLTs are binaries in which both members appear to be rotational variables (Stauffer et al. 2017; Rebull et al. 2018). Tokovinin & Briceño (2018) have used interferometry to resolve images of some T Tauri stars with non-commensurate periods into multiple components.

Koen (2015) showed that the amplitudes of both periodicities in the CVSO 30 light curve change over time. By implication, the relative flux contributions from the two stars also vary. This, along with the ubiquitous variability of the morphology of T Tauri star light curves, provides a natural explanation for changes in the visibility of the flux dips. Furthermore, if both stars belong to the T Tauri class, it is likely that both will show $H\alpha$ emission. If the emission is related to variability amplitude, then the measured line profile would also vary with time.

If the star is indeed a binary, then the results in Section 3 need to be revised somewhat. Assuming that the two stars have similar brightnesses, the luminosity of either star is $\sim 0.12 L_{\odot}$ and the bolometric magnitudes are 0.75 mag fainter, namely ~ 7 mag. The radius estimate is decreased by a factor of $1/\sqrt{2}$ to $R \approx 0.99 R_{\odot}$. The break-up rotation period is

$$P_b = 0.12 \sqrt{\frac{R^3}{M}} \text{ d},$$

where the radius and mass are in solar units. Briceño et al. (2005) supply two mass estimates of, respectively, 0.34 and 0.44 M_{\odot} ; with $R = 0.99 R_{\odot}$, $P_b = 0.18\text{--}0.20$ d, safely shorter than the ~ 0.4 d periods seen in the CVSO 30 light curves.

The parallax quoted in Section 3 translates into a distance to CVSO 30 of 350 ± 9 pc. The resolution limit of the speckle interferometry of Tokovinin & Briceño (2018) is 0.04 arcsec, which would imply a physical separation between binary components of 14 au at the distance of CVSO 30. Assuming a total binary mass of approximately $1 M_{\odot}$, the corresponding binary period would be 52 yr, and the orbital velocity 8 km s^{-1} . It may therefore be possible to test for binarity by either interferometric observations or high-precision radial velocity measurements taken over a few years.

ACKNOWLEDGEMENTS

The author thanks those maintaining the Simbad data base and the Vizier catalogue service in Strasbourg, France. The easy access to *TESS* photometry via the MAST portal and availability of the MIST bolometric correction tables are gratefully acknowledged. The paper benefitted from a well-informed referee's report.

REFERENCES

- Barnes J. W., Van Eyken J. C., Jackson B. K., Ciardi D. R., Fortney J. J., 2013, *ApJ*, 774, 53
- Briceño C., Calvet N., Hernández J., Vivas A. K., Hartmann L., Downes J. J., Berlind P., 2005, *AJ*, 129, 907
- Briceño C. et al., 2019, *ApJ*, 157, 85
- Chambers K. C. et al., 2016, preprint ([arXiv:1612.05560](https://arxiv.org/abs/1612.05560))
- Cutri R. M. et al., 2014, *Vizier Catalogue 2014yCat*, 2328
- Drake A. J. et al., 2014, *ApJS*, 213, 9
- Gaia Collaboration, 2018, *A&A*, 616, A1
- Gullbring E., Hartmann L., Briceño C., Calvet N., Muzerolle J., 1998a, in Donahue R. A., Bookbinder J. A., eds, *ASP Conf. Ser. Vol. 154, Cool Stars, Stellar Systems and the Sun*. Astron. Soc. Pac., San Francisco, p. 1709
- Gullbring E., Hartmann L., Briceño C., Calvet N., 1998b, *ApJ*, 492, 323
- Howarth I. D., 2016, *MNRAS*, 457, 3769
- Johns-Krull C. M. et al., 2016, *ApJ*, 830, 15
- Kamiaka S. et al., 2015, *PASJ*, 67, 94
- Koen C., 2015, *MNRAS*, 450, 3991
- Lee C.-H., Chiang P.-S., 2018, *ApJ*, 852, L24

- Onitsuka M., Fukui A., Narita N., Hirano T., Kusakabe N., Ryu T., Tamura M., 2017, *PASJ*, 69, L2
- Pecaut M. J., Mamajek E. E., 2013, *ApJS*, 208, 9
- Pecaut M. J., Mamajek E. E., Bubar E. J., 2012, *ApJ*, 756, 154
- Raetz S. et al., 2016, *MNRAS*, 460, 2834
- Rebull L. M., Stauffer J. R., Cody A. M., Hillenbrand L. A., David T. J., Pinsonneault M., 2018, *AJ*, 155, 196
- Ricker G. R. et al., 2015, *J. Astron. Telesc. Instrum. Syst.*, 1, 014003
- Schafly E. F. et al., 2016, *ApJ*, 821, 78
- Schmidt T. O. B. et al., 2016, *A&A*, 593, A75
- Skrutskie M. F. et al., 2006, *AJ*, 131, 1163
- Stauffer J. et al., 2017, *AJ*, 153, 152
- Stauffer J. et al., 2018, *AJ*, 155, 63
- Tanimoto Y. et al., 2020, *PASJ*, 72, 23
- Tokovinin A., Briceño C., 2018, *AJ*, 156, 138
- Van Eyken J. C. et al., 2012, *ApJ*, 755, 42
- Yu L. et al., 2015, *ApJ*, 812, 48
- Zhan Z. et al., 2019, *ApJ*, 876, 127

This paper has been typeset from a \TeX/L\TeX file prepared by the author.